frontiers in Marine Science

TYPE Original Research
PUBLISHED 19 August 2026
DOI 10.3389/fmars.2026.1920990

Check for updates

OPEN ACCESS

EDITED BY
Eric Chassignet,
Florida State University, United States

REVIEWED BY
Andrew Poje,
The City University of New York,
United States
Yueyang Lu,
Massachusetts Institute of Technology,
United States

*CORRESPONDENCE
Lilli Enders
lilli.enders@whoi.edu

RECEIVED 26 June 2026
REVISED 21 July 2026
ACCEPTED 27 July 2026
PUBLISHED 19 August 2026

CITATION
Enders L, Kwon Y-O and Frankignoul C (2026) Non-stationarity in the NAO-Gulf Stream interannual relationship. *Front. Mar. Sci.* 13:1920990. doi: 10.3389/fmars.2026.1920990

Non-stationarity in the NAO-Gulf Stream interannual relationship

Lilli Enders[1,2*], Young-Oh Kwon[1] and Claude Frankignoul[1,3]

[1]Department of Physical Oceanography, Woods Hole Oceanographic Institution, Woods Hole, MA, United States, [2]MIT– WHOI Joint Program in Oceanography/Applied Ocean Science & Engineering, Cambridge, MA, United States, [3]Le Laboratoire d'Océanographie et du Climat: Expérimentations et Approches Numériques (LOCEAN), Sorbonne Université/IRD/CNRS/MNHN, Paris, France

The North Atlantic Oscillation (NAO) is widely recognized as a primary driver of the Gulf Stream (GS) path variability on interannual to decadal timescales. While the canonical view holds that the GS path responds to the NAO in a temporally stationary and approximately linear manner, we show that the sign and strength of the NAO-GS relationship vary markedly through time. Using satellite altimetry, atmospheric reanalysis, and a wind-driven, two-layer ocean model, we investigate the temporal evolution and dynamical origins of this non-stationarity in the relationship between the NAO and the meridional position of the separated GS throughout the altimetry era (1993-2023). Lead-lag analysis of the full record shows a significant, positive correlation between the NAO and GS position when the NAO leads by 3–20 months, with the maximum correlation occurring at a lag of 8 months. However, moving-window correlations demonstrate pronounced modulation of this relationship through time, with transitions from strong positive correlations to weak or reversed correlations. This behavior is reproduced by the wind-driven model, indicating that wind forcing plays a dominant role in driving the observed non-stationarity in the NAO-GS relationship. Analysis of sea level pressure variability reveals substantial shifts in the spatial structure of the NAO. The transition from positive to weakly negative NAO–GS correlation coincides with southwestward shifts of the subtropical high and subpolar low, consistent with changes in the geometry of the associated wind stress curl forcing over the GS region and intergyre boundary. These results suggest that the sensitivity of the GS to atmospheric variability depends strongly on the spatial structure of the forcing, rather than solely its magnitude, and highlight the importance of accounting for non-stationarity when interpreting and predicting GS variability and its impacts on regional climate, sea level, and marine ecosystems.

KEYWORDS
Gulf Stream, interannual variability, non-stationarity, North Atlantic Oscillation, ocean–atmosphere interaction, wind-driven circulation

1 Introduction

The Gulf Stream (GS), the western boundary current of the North Atlantic, serves as a conduit for the poleward transport of heat, salt, and nutrients, and thus plays a critical role in regulating global climate as well as regional ecosystems. After its separation from the continental shelf near Cape Hatteras, North Carolina, the GS flows into deep waters as a vigorously meandering free jet. The separated GS is characterized by two dynamically distinct modes of variability: wavelike fluctuations associated with meandering, and large-scale meridional shifts in the latitude of its mean path (Lee and Cornillon, 1995; Pérez-Hernández and Joyce, 2014). The meridional fluctuations in the position of the GS (i.e., GS path variability) represent the dominant mode of variability in the region of the separated GS (55°- 70°W) at interannual to decadal time scales (Gangopadhyay et al., 2016). The GS path variability modulates heat, salt, and momentum distributions in the North Atlantic, ultimately affecting regional climate, ocean circulation, and ecosystem dynamics. Enhancing dynamical understanding and predictability of the GS path variability and its drivers is therefore critical for improving forecasts of regional climate extremes (Joyce et al., 2019), projecting sea level rise along the Northeast U.S. coast (Hong et al., 2000), and assessing ecosystem shifts in a changing climate (Nye et al., 2011).

Various mechanisms have been proposed to explain the low-frequency modulations in the path of the separated GS. Previous studies have addressed the roles of variable equatorward transport of Labrador Sea Water in the Deep Western Boundary Current (Hameed and Piontkovski, 2004; Joyce et al., 2000; Pena-Molino and Joyce, 2008; Zhang and Vallis, 2007), the dynamics of the crossover between the Deep Western Boundary Current and the GS (Spall, 1996), westward propagation of long baroclinic oceanic Rossby waves (Gangopadhyay et al., 1992; Silver et al., 2021), and the influence of a number of large-scale climate modes, including the North Atlantic Oscillation (NAO; Frankignoul et al., 2001; Joyce et al., 2000; Kwon et al., 2010; Paolini et al., 2024; Taylor and Gangopadhyay, 2001), the Atlantic Meridional Mode (Wolfe et al., 2019), and the El Niño-Southern Oscillation (Sanchez-Franks et al., 2016; Taylor and Stephens, 1998). The NAO, which is the leading mode of atmospheric variability over the North Atlantic (Hurrell, 1995), has in particular been rigorously linked to the path of the GS. In this work, we focus primarily on the influence of the NAO on the latitudinal position of the GS.

The NAO is thought to exert control over the path of the GS on interannual to decadal timescales through both wind- and buoyancy-driven mechanisms (Figure 1). Anomalous winds associated with NAO drive meridional shifts in the wind stress curl field and changes in its configuration: positive phases are associated with a northward shift and stronger tilt of the zero wind stress curl line and associated storm track, and a strengthening of the jet stream, while negative phases are associated with a more southerly and zonal configuration in the zero wind stress curl line and the storm track (Marshall et al., 2001). These changes alter the position of the GS through Ekman pumping both locally (i.e., over the region of the separated GS and recirculation gyres), and remotely (i.e., in the central and eastern North Atlantic through the excitement of barotropic and baroclinic Rossby waves, which propagate westward), as schematically depicted in Figure 1a.

Previous studies point to these wind-driven response mechanisms to explain observed positive correlations between NAO and the GS, with the position of the GS varying in a relatively linear manner with respect to phase and intensity of the NAO (e.g., Marshall et al., 2001; Silver et al., 2021; Taylor and Gangopadhyay, 2001). Changes in the GS position are observed to lag changes in the atmospheric circulation by less than one year, in some studies (Joyce et al., 2000), and by 2–3 year, in others (Hameed and Piontkovski, 2004; Paolini et al., 2024). The time lags are often attributed to the crossing time of fast barotropic and slow baroclinic Rossby waves generated in the interior North Atlantic. Despite its frequent invocation, the precise impact of Rossby wave propagation on the GS position remains unclear. In particular, linear theory predicts first-baroclinic Rossby wave phase speeds of only 1.5 cm/s at 40°N (Chelton et al., 1998), implying transit times of approximately 11 years from the eastern basin (10°W) and 6 years from the central basin (40°W) to the western boundary, substantially longer than the observed NAO-GS lag. Even using empirically derived propagation speeds of 3–5 cm/s at mid-latitudes (Chelton and Schlax, 1996), the corresponding crossing times remain on the order of several years.

Changes in wind patterns associated with NAO are also accompanied by changes in the air-sea heat fluxes that drive

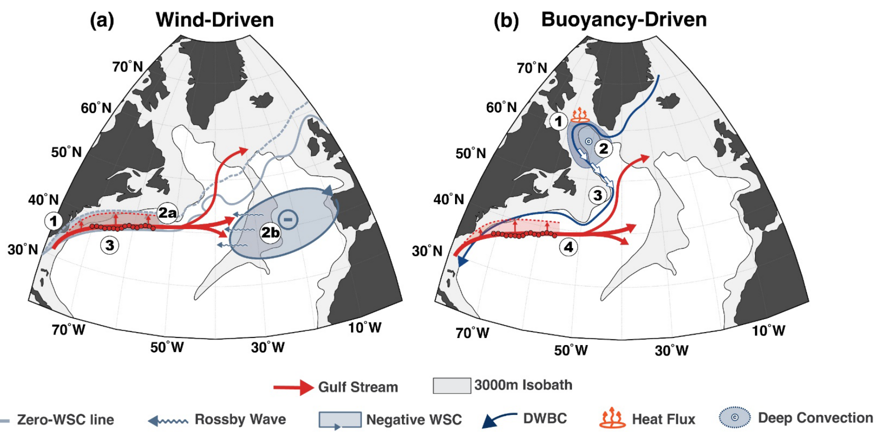

FIGURE 1
Schematic of Gulf Stream response mechanisms to atmospheric forcing in the positive NAO phase, as described in Marshall et al. (2001). **(a)** Wind-driven response: (1) Zero-wind stress curl line shifts northward under positive NAO forcing, (2a) locally (over the GS corridor), the GS path follows the zero wind stress curl line, (2b) remotely (in the central and eastern basin) anomalous negative wind stress curl excites barotropic and baroclinic Rossby waves, which propagate westward as sea level anomalies, (3) GS shifts northward in response. **(b)** Buoyancy-driven response: (1) Positive NAO forcing enhances heat flux out of the ocean in the Labrador sea, leading to (2) enhanced deep convection in the Labrador Sea, which in turn leads to (3) enhanced equatorward transport of the Deep Western Boundary Current, (4) shifting the GS path at its separation point from the coast, as it crosses underneath it.

anomalous thermohaline circulation, thus impacting the GS position (Hameed and Piontkovski, 2004; Joyce and Zhang, 2010; Marshall et al., 2001). When NAO is in its positive phase, enhanced surface heat loss from the ocean is observed northward of ~ 45°N (inducing negative sea surface temperature anomalies in this region), and reduced air-sea fluxes are observed between ~ 30°N and 45°N (inducing positive sea surface temperature anomalies in this region; Cayan, 1992; Hurrell and Deser, 2009). Sustained enhancement of cooling in the subpolar North Atlantic, particularly in the Labrador Sea, results in a strengthening of the thermohaline circulation and an increase in the export of Labrador Sea Water in the Deep Western Boundary Current (Figure 1; Dickson et al., 1996; Marshall et al., 2001; Talley, 1996). The resulting circulation adjustment is expected to influence the GS with a lag of 5–10 years, reflecting the advective timescale of Labrador Sea Water anomalies within the Deep Western Boundary Current (Le Bras, 2023; Pena-Molino and Joyce, 2008).

Besides the forcing mechanism, the details of the lead-lag relationship between the GS and NAO, including the strength of the correlation and the lag at which NAO leads the GS, may be sensitive to several other factors, including the GS and NAO indices used, the time period and/or season studied, and methods employed for filtering and smoothing time series. Recent evidence suggests that in addition to sensitivity related to these choices, signals consistent with physically meaningful non-stationarity in the GS-NAO relationship may exist, particularly at decadal timescales. Paolini et al. (2024), for example, observe non-stationarity in the lead-lag relationship between the NAO and latitudinal shifts in the GS temperature front. Using yearly winter mean GS temperature front indices based on sea surface temperature gradients, they find that the NAO tends to lead meridional shifts in the GS by 3 years during 1972–1990, but by 2 years during 1990–2018. This finding is attributed to a lack of Rossby wave propagation in the latter period, leading to a faster response of the GS than in the preceding years, although it is not clear why the Rossby wave propagation was active only in the early period.

In this study, we seek to extend these results to understand (1) whether the NAO-GS relationship is also non-stationary on shorter (interannual) timescales, and (2) whether non-stationarity extends to the sign and strength of the NAO-GS correlation, in addition to the lag of maximum correlation.

2 Data and methods

2.1 Observational and reanalysis datasets

Observed sea level anomalies from satellite altimetry and surface variables from an atmospheric reanalysis are used in our study. Satellite derived gridded sea level anomaly data, along with mean dynamic topography (MDT) from the TOPEX/Poseidon joint mission, were downloaded from the Archiving, Validation and Interpretation of Satellite Oceanographic data (AVISO) data center for the years 1993-2023. The anomaly in sea level is computed relative to a 20-year climatological reference period (1993-2012). Monthly averaged sea level anomaly data at a horizontal resolution of 0.25° was downloaded for the North Atlantic region (90°W-0°,10°-70°N). The mean seasonal cycle was defined as the average of each month over the time series at each grid cell and was removed from each variable at each point. A linear trend was also removed from the time series of sea level anomaly at each grid point.

Other surface variables used in our study, namely sea level pressure, wind stress, wind stress curl, and surface heat fluxes, were downloaded from the European Centre for Medium-Range Weather Forecasts (ECMWF) Reanalysis v5 (ERA5; Hersbach et al., 2020). The wind stress curl was computed from the eastward and northward components of surface wind stress using Stokes' Theorem. The surface heat fluxes include the short wave and long wave radiative fluxes, as well as the turbulent (i.e., sensible and latent) heat fluxes. The climatological mean (computed for reference period 1993-2012) has been removed from each variable. Wind stress and wind stress curl as well as the surface heat fluxes were deseasonalized and linearly detrended following the method described in the preceding paragraph.

2.2 Two-layer model output

To isolate the wind-driven component of variability, we consider output from a two-layer, wind forced shallow water ocean model developed by Yang (2015). The model is forced only by the ERA5 wind stress, and employs realistic topography from the Earth Topography Five-Minute Grid (ETOPO5) bathymetry data (which has a horizontal resolution of 5 minutes of latitude and longitude). The model includes two active layers, such that the barotropic and first baroclinic modes are active. Outcropping of the lower layer and grounding of the upper layer are permitted by the model configuration (i.e., the thickness of each layer is allowed to go to zero). The model covers the North Atlantic domain (100°W-20°E, 2°S-80°N) with a horizontal resolution of 0.25° in latitude and longitude. No-slip and no-normal flow boundary conditions are applied. Monthly mean output from the model is used in this study. Forty years of model data (1979-2019) are available. The model is governed by Equations 1a-d:

$$\frac{\partial \vec{u_1}}{\partial t} + \vec{fk} \times \vec{u_1} = -g\nabla\eta_1 - A\,\nabla^4\,\vec{u_1} - (1 - H(h_2))\vec{F_1} + \frac{\overrightarrow{\tau_{wind}}}{\rho_o h_1} \tag{1a}$$

$$\frac{\partial \vec{u_2}}{\partial t} + \vec{fk} \times \vec{u_2} = -g\nabla\left(\eta_1 + \frac{\Delta\rho}{\rho_2}\eta_2\right) - A\,\nabla^4\,\vec{u_2} - \vec{F_2} - (1 - H(h_1))\frac{\overrightarrow{\tau_{wind}}}{\rho_2 h_2} \tag{1b}$$

$$\frac{\partial \eta_1}{\partial t} + \nabla \cdot (h\vec{u_1} + h\vec{u_2}) = 0 \tag{1c}$$

$$\frac{\partial h_2}{\partial t} + \nabla \cdot (h\vec{u_2}) = 0 \tag{1d}$$

where the velocity and thickness of each layer (n = 1,2) are given by u_n, v_n, and h_n, respectively, H is a Heaviside Step Function ($H(h_i)$ =

1 if $h_i > 0$, $H(h_i) = 0$ if $h_i \leq 0$), η_1 is the sea level anomaly, η_2 is the height of the interface anomaly, $A = 10^{12} m^4 s^{-1}$ is a biharmonic viscosity, $\overrightarrow{F_n} = \frac{\lambda |\overrightarrow{u_n}| \overrightarrow{u_n}}{h_n}$ is the bottom drag, and $\Delta\rho = 1.5 kgm^{-3}$ is the density difference between the two layers. A complete description of the model composition can be found in Yang (2015).

In this study, the two-layer model provides a method for the isolation of the wind-driven component of sea level variability, since there is no buoyancy forcing for this model. The model has been successfully employed for a host of applications, including simulating seasonal variability of bottom pressure in the North Pacific (Chen et al., 2023), along-shelf flow on the Middle-Atlantic Bight (Yang and Chen, 2021), and the wind-driven variability of the Atlantic Meridional Overturning Circulation (Yang, 2015). In each of these cases, the two-layer model produces results in good agreement with observational data and reanalysis.

2.3 Gulf Stream index

An index of the separated GS's meridional position is constructed using sea level anomaly. The procedure for deriving this index is as follows: standard deviation of sea level anomaly at each grid point is computed over the study region, and values are summed along each isoline of mean sea level. The isoline with the maximum standard deviation is selected as the approximate mean path of the GS. Once this mean path has been defined, an array of points is selected following the isoline. The points are placed every 1° in longitude between 55° and 70°W for a total of 16 points. sea level anomalies are then averaged over this 16-point array at each monthly time step to form the GS index time series. Because the Gulf Stream coincides with a sharp gradient in mean sea surface height, meridional shifts of the current alter the local sea level relative to the climatological mean. Positive (negative) sea level anomaly corresponds to a northward (southward) displacement of the Gulf Stream from its mean path, making the averaged sea level anomaly along the mean Gulf Stream path a proxy for fluctuations in its meridional position.

This method is similar to that introduced by Pérez-Hernández and Joyce (2014), who developed a GS index based on 16 points, which correspond to the latitude of maximum standard deviation at each longitude in the satellite-derived sea level anomaly field. We find that restricting these points to a single isoline allows the method of Pérez-Hernández and Joyce (2014) to be effectively applied to a variety of model output fields, as well as observations, by ensuring a cohesive path and eliminating apparent meridional 'jumps' in the mean path, which are sometimes observed when deriving the GS path from model sea surface height fields using the method of Pérez-Hernández and Joyce (2014). The method described here produces an observational time series in good agreement with that produced using the 16-point index described by Pérez-Hernández and Joyce (2014), (r = 0.93, for unfiltered monthly time series).

Between 55° and 70°W, the mean path of the observed separated GS defined using this method is zonally tilted (Figure 2), such that the current flows northeastward between approximately 38°N (at 70°W) and 40°N (at 55°W). At approximately 63°W, the longitude where the GS typically intersects the New England Seamount Chain, the mean path of the GS is diverted northward by approximately one degree of latitude, before continuing its northeastward trajectory. This is consistent with existing literature, including observational analysis by Chassignet et al. (2023).

2.4 North Atlantic Oscillation index

An index of the NAO was constructed by computing the leading Empirical Orthogonal Function (EOF) and corresponding principal component time series of monthly mean sea level pressure anomaly over the North Atlantic basin (20°-80°N, 90°W-40°E; Figure 3b), weighted by the squared root of cosine of latitude ($\sqrt{cos(\theta)}$). As described in Section 2.1, the sea level pressure anomaly was first deseasonalized and linearly detrended prior to EOF calculation. The principal component time series are normalized and the EOF pattern is obtained by regression on the normalized principal component time series.

2.5 Statistical practices

Indices were low-pass filtered using a Butterworth filter applied to monthly time series. A cutoff period of 13 months was used to remove the annual and subannual variability, while retaining lower frequency signals.

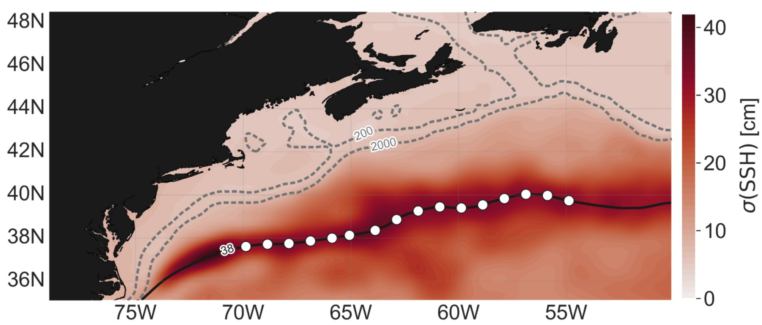

FIGURE 2
Path of mean Gulf Stream in observations using full time series (1993-2023). Shading is standard deviation of monthly sea surface height ($\sigma(SSH)$) from the full observational record (1993–2023) after the climatological monthly means and linear trend are removed at each grid point (Section 2.1). Solid black line represents isoline along which maximum standard deviation is found (39cm). Dots represent the points along the isoline that are averaged to calculate the Gulf Stream Index time series. Gray dashed lines represent 200m and 2000m isobaths.

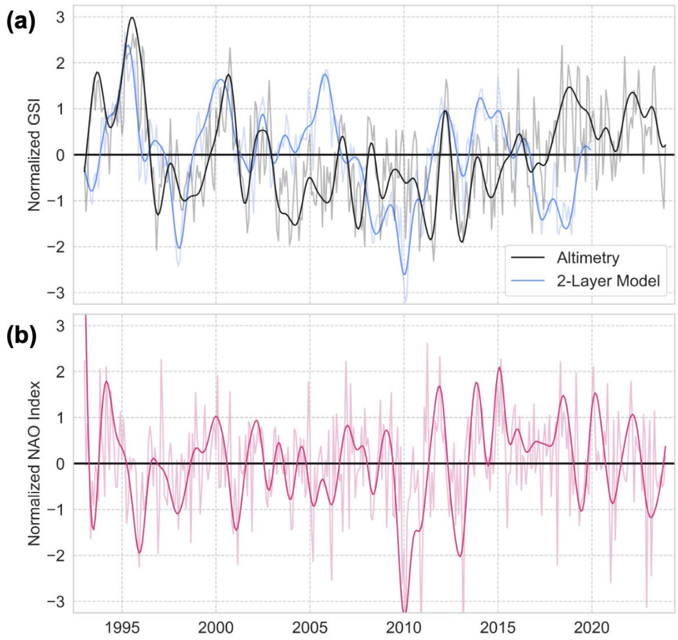

FIGURE 3
(a) Time series of Gulf Stream position index (GSI) in observations (black) and two-layer model (blue). **(b)** Time series of NAO index. A low-pass, Butterworth filter with a cutoff frequency of 13 months has been applied to each time series (solid lines). The unfiltered, monthly time series appear in faint lines behind the filtered time series.

The statistical significance of each correlation is tested against a null hypothesis of no correlation at a confidence level of 95%. A confidence interval is constructed using a phase scrambling approach in the frequency domain, repeated in a bootstrapping framework with 10,000 resampling instances, following the method described by Ebisuzaki (1997).

3 Results

3.1 Non-stationarity in the observed NAO-GS relationship

The observed GSI time series (Figure 3a, faint black line) is characterized by slow, coherent oscillations between northward and southward displacements of the current. During the early portion of the record (1993–2001), the GS is predominantly positioned north of its mean latitude. Between 2002 and 2015, the current resides primarily south of its mean position. The low-pass filtered index (Figure 3a, solid black line) shows the GS at its northernmost point in 1995, and its southernmost point in 2013, marking the extrema of the observed variability over the record. Spectral analysis exhibits pronounced energy in the 2–4 year band, indicative of enhanced interannual variability (Supplementary Figure 1). Consistent with this, the autocorrelation structure of the linearly detrended GSI highlights a damped quasi-periodic signal (Supplementary Figure 2a), reflecting repeated transitions between northward (positive) and southward (negative) configurations, superposed on a slower decay.

The low-pass filtered GSI and NAO index are significantly, positively correlated (at the 95% confidence level) when the NAO leads the GS position by 3 to 20 months (Figure 4, black line). The maximum positive correlation ($r = 0.17$ and $r = 0.38$ for the unfiltered and filtered time series, respectively) between the indices occurs in both cases when the NAO leads the GSI by 8 months (i.e., a positive NAO precedes a northward shift in the GS path by 8 months). A weaker, secondary cluster of positive correlation is noted when NAO leads the GS by 40–43 months (approximately 3.5 years). No significant correlations are observed at positive lags, where the GS path leads the NAO index. This indicates that, at interannual timescales, variability in the GS path is not exerting significant control over the NAO. Alternatively, the GS impact on the NAO may be confined to certain season (e.g., winter), thus the correlation using all months may not exhibit the signal. The timescale of the maximum correlations between the observed GS position and NAO indices (8 months) is within the range observed in some previous studies (e.g., Frankignoul et al., 2001; Joyce et al., 2000), while the longer timescale (3.5 years) is broadly consistent with others (e.g., Paolini et al., 2024). There is no significant correlation between the GS position and the East Atlantic Pattern (EAP), the second mode of atmospheric variability, so we only focus on the links with NAO.

The relatively fast response of the ocean circulation to changes in the atmosphere indicates that wind forcing may be a primary driver of the GS position in response to shifts in NAO phase. The short time lag is inconsistent with adjustment dominated by slow baroclinic Rossby waves propagating from the interior subtropical basin, which would imply a response time of several years. Instead, the observed lag is more consistent with a combination of fast

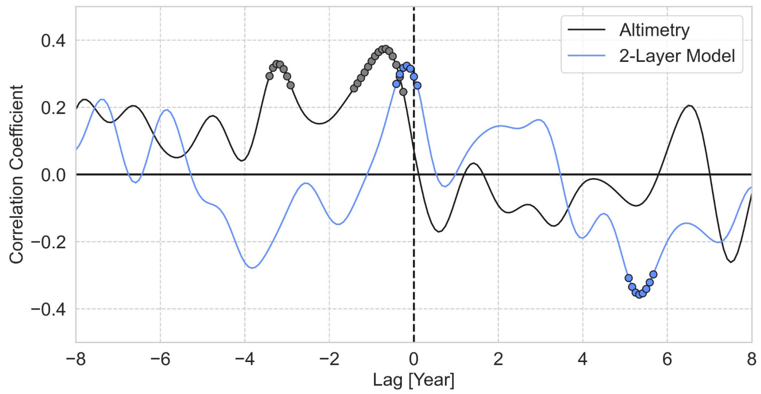

FIGURE 4
Lead-lag relationship between the low-pass filtered NAO and GS indices from observational data (black) and two-layer model output (blue). Dots indicate correlation is significant at the 95% confidence level. At negative lags, the NAO leads the GSI.

barotropic adjustment and locally excited first-baroclinic mode processes.

To assess potential non-stationarity of the fast NAO-GSI relationship, a moving window correlation of the indices is computed (Figure 5, black line). The lag of the GSI is fixed at its maximum, positive value for the full time series (-8 months; Figure 4), and a sliding window of 48 months is applied to the low-pass filtered time series of GSI and NAO index. An NAO-GSI correlation is then computed for each window. The time evolution and magnitude of the moving correlation signal are robust to our choices of window size and lag between NAO and GSI. Window sizes of 12- to 108-months and lags of 4- to 12-months were tested (Supplementary Figures 3, S4).

The moving-correlation time series indicates a dependence of the NAO-GSI correlation on the time period of interest (i.e., non-stationary behavior in the NAO-GSI correlation). Near the beginning of the record (1997–06 to 2001-10), a strong, positive correlation between the two indices is observed (yellow shading in Figure 5). This is followed by a period of weak, mostly insignificant, negative correlation between the indices, such that a positive NAO phase is associated with a southward shift in the GS path (2004–02 to 2008-06, gray shading in Figure 5), before returning to a state of weak, albeit insignificant, positive correlation (2009–01 to 2014-11). The mechanisms underlying these variations in correlation strength are investigated in Section 3.3. Note that the moving correlation calculation includes 2 years prior and 2 years after these periods (indicated by the dashed vertical lines in Figure 5), since each moving correlation is assigned to the center of the corresponding moving window.

This non-stationarity primarily reflects variability at interannual time scales, since low-pass filtering of the NAO and GS indices removes annual and subannual variability, and the dominant NAO-GSI relationship occurs at subannual lags. To assess the timescales contributing to the non-stationarity, we repeated the moving-correlation analysis using a range of low-pass filter cutoffs (cutoff periods of 13-, 24-, 36-, 60-, and 120-months were tested; not shown). The timing and magnitude of the transitions between positive and negative NAO-GSI correlation were largely preserved when variability with periods shorter than approximately 2–5 years was retained, but became substantially weaker when only lower-frequency variability was considered. This indicates that the observed non-stationarity is primarily associated with modulation of

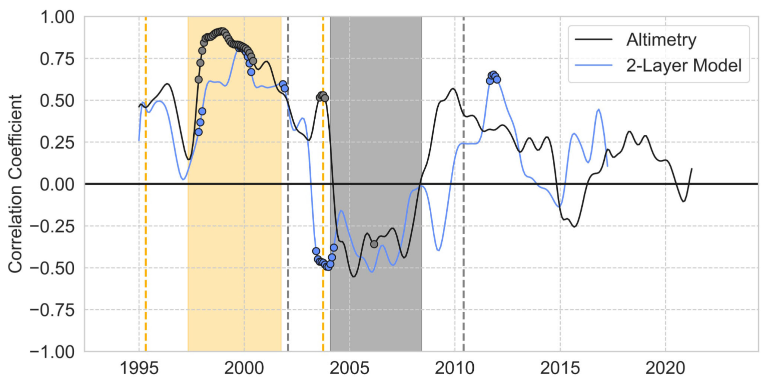

FIGURE 5
Moving correlation between GSI and the NAO for altimetric observations (black) and two-layer model output (blue). A window size of 48-months is applied to calculate the moving correlation. The lag of the Gulf Stream is held constant at the value of the maximum NAO-GSI correlation for the whole time series (-8 months and -2 months for the observational and model time series, respectively). Time axis represents the center of each 48-window (ex. '1995-01' value represents the correlation for 1993–01 to 1996–12 NAO values). Shaded areas represents Period 1 (1997–06 to 2001-10; yellow) and Period 2 (2004–02 to 2008-06; gray). Dashed vertical lines represent the extremities of points included in each period, i.e., ± 2 years.

the interannual component of the NAO-GSI relationship, rather than arising solely from variability at decadal timescales.

3.2 Role of wind forcing inferred from two-layer model

Analogous analysis of the two-layer, wind-driven model simulation provides additional context for the interpretation of the observed results. The mean path of the two-layer model is, on average, approximately 1° further northward than the mean path of the observations (not shown). This results from northward bias in the separation of the GS from the coast, which is a well-documented issue in numerical models, particularly with non-eddy-resolving resolutions. The lack of buoyancy forcing in the model may also contribute to bias in the separation location, as buoyancy-driven aspects of the circulation (including strength of the Deep Western Boundary Current) are thought to influence the separation of the GS near Cape Hatteras (Spall, 1996).

The model GSI time series exhibits variability that is comparable to that of the observed index (blue curve in Figure 3a). Energy in the power spectrum (Supplementary Figure 1) is distributed across frequencies, with the strongest signals appearing at interannual to decadal time scales. The two-layer model is lower in energy than observations across the frequency spectrum, with the largest differences occurring at high frequencies (periods less than 2 years). The model autocorrelation function (Supplementary Figure 2b) also has a longer e-folding time scale than the observational case (Supplementary Figure 2a; 12 months vs. 3 months), indicating that the model GSI holds longer memory. This may be a result of the active eddies present in the observational field, which create higher frequency noise in the sea level time series.

The observed and modeled GSI time series are moderately but significantly correlated at the 95% confidence level ($r = 0.21, 0.24$ for unfiltered and filtered time series, respectively, with maximum correlation occurring at zero lag), agreeing particularly well in the early part of the record (1993-2002, $r = 0.49, 0.60$ at zero lag for the unfiltered and filtered time series, respectively). This agreement may indicate that the variability in the GS position is primarily wind-driven in the first portion of the record.

The two-layer model GSI and the NAO index are significantly, positively correlated at -1 to 5-month lags (Figure 4, blue line). The maximum correlation between the indices is observed where the NAO leads the GS position by 2 months. These results are qualitatively similar to those described for the observational GSI, although the maximum lag is slightly longer in the observational case (8 months). The secondary correlation peak observed when the NAO leads the GS by approximately 3–4 years is, however, absent from the wind-driven model simulation, suggesting that it may reflect buoyancy-driven adjustment processes.

The application of a 48-month moving window with a fixed lag of -2 months successfully reproduces the key features identified in the observational result, with some temporal offset reflecting the faster response time in the model (Figure 5, blue line). A significant, positive, correlation between the model GSI and NAO is noted in the first period of the record (1997-2001), followed by a reversal in the sign of the correlation (with mostly insignificant correlations) between 2004 and 2008. The signal then returns to a weakly positively correlated state. Consistent with the observed case, the time evolution and magnitude of the moving correlation signal are robust to our choices of window size and lag between NAO and GSI (Supplementary Figures 5, S6).

The ability of the two-layer model to successfully reproduce the non-stationary behavior in the observed NAO-GSI relationship suggests that this apparent non-stationarity is primarily wind-driven, as the two- layer model includes only wind forcing. When considered alongside the short time lags, which indicate a dominant role for local or barotropic processes, this points to wind variability being communicated to the GS through rapid barotropic or local adjustment mechanisms.

3.3 Mechanisms for modulation of the gulf stream path

To identify the dynamical differences between periods where the GS-NAO relationship is positive and periods where it is weakly negative, we define two reference periods. Period 1 (1997–06 to 2001-10) covers the strongest positive correlations observed in the time series. This period represents the 'canonical' relationship between the GS and NAO. Period 2 (2004–02 to 2008-06) covers the portion of the observational record where the sign of the NAO-GS relationship reverses.

3.3.1 Differences in the spatial structure of atmospheric forcing

Spatial patterns of the first two leading EOFs derived from the low-pass filtered sea level pressure for the full record (1993-2023) present a classical picture of the leading modes of atmospheric variability over the North Atlantic (Figures 6a, d). The leading mode of sea level pressure, which explains nearly half of the total variance, is the NAO, with two well-defined centers of action (i.e., a subpolar low, and a subtropical high; Figure 6a). The centers of action are located over the eastern portion of the basin, with the subpolar low centered east of Iceland, and the subtropical high centered over the Azores. The boundary between the low pressure center over the subpolar gyre and the high pressure center over the subtropical gyre extends across the basin near 50°N. The second mode of sea level pressure, which explains about 20% of the total variance, has a single positive pressure center in the eastern-central basin near 52°N (Figure 6d). The magnitude of the EOF 2 loadings are comparable to those of EOF 1. This mode is often referred to as the EAP.

Comparison of the EOF patterns for Periods 1 and 2 reveal significant changes in the spatial structure of the leading modes of atmospheric variability between the two reference periods (Figure 6). The sea level pressure EOF patterns of Period 1 closely resemble those derived from the full record, with the first mode being a NAO, and the second mode being an EAP (Figures 6b, e). The loading patterns of the first two modes notably shift in Period 2 when compared to Period 1 (Figures 6c, f). While EOF 1 remains an 'NAO-like' pattern (i.e., a center of low pressure in the subpolar basin and a center of high pressure in the subtropical basin), both

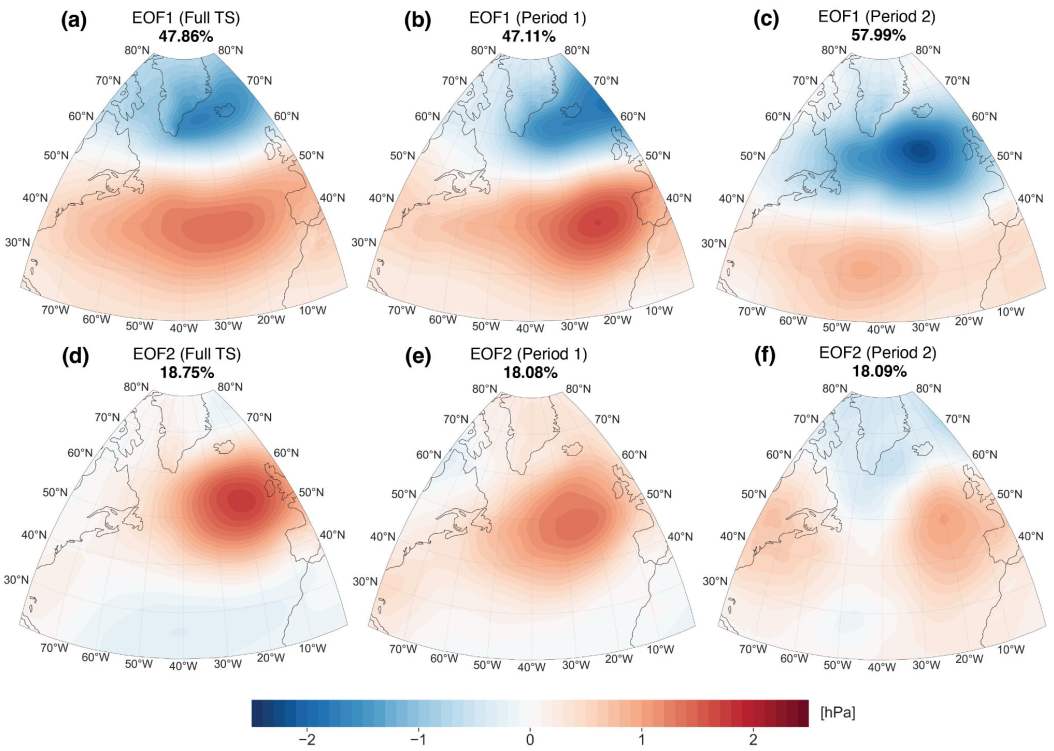

FIGURE 6
EOFs 1 (top row) and 2 (bottom row) of monthly ERA5 sea level pressure over the North Atlantic (20°- 80°N, 90°W-0) for full record [**(a, d)**; 1993–01 to 2023-12], Period 1 [**(b, e)**; 1997–06 to 2001-10], and Period 2 [**(c, e)**; 2004–02 to 2008-06]. Percent variance explained by each EOF is expressed in subplot titles.

centers of action appear to exhibit profound southwestward shifts. The boundary between the high and low pressure centers shifts south by more than 10° of latitude compared to Period 1. In addition, both the subtropical high and subpolar low shift westward towards the central basin, such that the pattern also bears some resemblance with a northward shifted, negative phase of the EAP. The percentage of the total variance explained by the EOF 1 is substantially higher (~58%) than that for Period 1 or the full record (~47%). While the second mode of Period 2 still has a positive center of action over the eastern portion of the basin, a zonally distributed tripole pattern emerges (Figure 6f), which does not resemble the EAP.

The temporal evolution of the centers of action further quantifies these shifts. A 48-month moving window is applied to the sea level pressure data, and the EOFs are computed for each 48-month moving window. For each window, a spatial correlation between the full-period EOF 1 (NAO) and EOF 2 (EAP) fields is performed to determine whether each EOF is 'NAO-like' or 'EAP-like'. While the first mode is typically 'NAO-like' (i.e., $r > 0.8$ for spatial correlations), there are cases in which EAP is identified as the leading mode, and NAO the second mode. The majority of these cases are identified in the transition period between Period 1 and Period 2 (2000–11 to 2004-01). In all windows, NAO is either the leading mode or the second mode.

Shifts in the subpolar and subtropical centers of action are then examined in the NAO-like EOF fields for each window by identifying their latitude and longitude (Figure 7). This analysis reveals that the two centers of action simultaneously shift southwestward beginning in 2001, coincident with the reversal in the NAO-GS relationship noted in Figure 5. While the latitudinal positions of the centers of action return to their mean state near the end of Period 2, the westward shifts in the longitudinal positions of the centers of action persists throughout the record. The systematic southwestward shifting of NAO's subtropical high and subpolar low, which corresponds with the transition between Period 1 (in which NAO and the GS position are positively correlated) and Period 2 (in which the NAO and GS position are weakly/negatively correlated), may suggest that the observed changes in the positioning of atmospheric forcing contribute to modulating the oceanic response.

3.3.2 Impact of changes in NAO on the Gulf Stream position

To understand how the changes in the spatial structure of NAO described in the preceding section translate into dynamical forcing of the GS, we examine regressions of wind stress curl anomalies onto the NAO and GS indices.

During Period 1, the regression of wind stress curl anomalies onto the NAO index reveals the canonical basin-scale forcing pattern associated with a positive NAO phase (Figure 8a). Enhanced anticyclonic wind stress curl anomalies extend across the subtropical-subpolar gyre boundary, while cyclonic anomalies intensify farther north in the subpolar basin, forming the characteristic intergyre-gyre structure described by Marshall et al. (2001). At the local scale, an organized pattern of anticyclonic (i.e.,

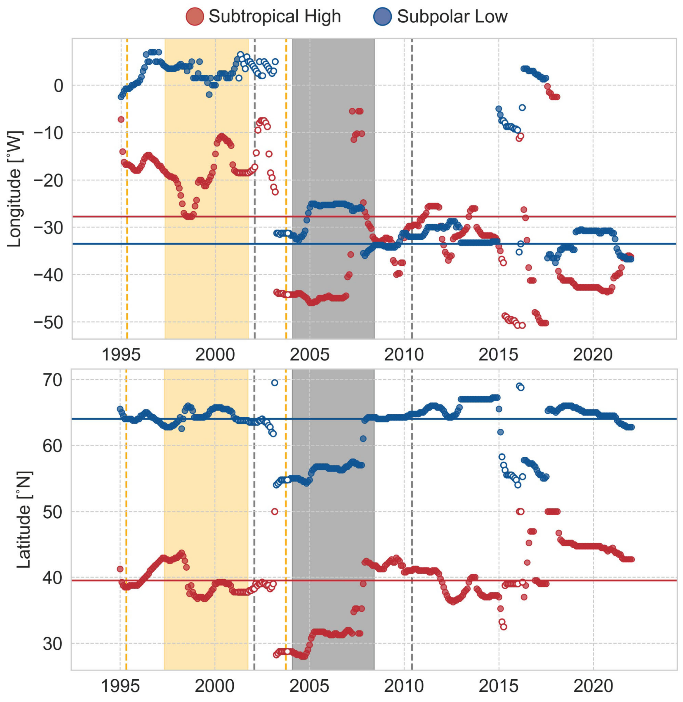

FIGURE 7
Time series of NAO subtropical high and subpolar low longitude (top) and latitude (bottoms) for each of the 48-month window, as described in Figure 6. Longitude and latitude values represent the position of maximum and minimum pressure anomalies for the subtropical high and subpolar low, respectively. Horizontal dashed line represents the mean position of the subpolar low and subtropical high for the full period (1993–2023). Shaded areas represent Period 1 (1997–06 to 2001-10; yellow) and Period 2 (2004–02 to 2008-06; gray). Dashed vertical lines represent the extremities of points included in each period, i.e., ± 2 years.

negative) wind stress curl anomalies extends along the mean path of the separated GS (Figure 9a), flanked by weaker, cyclonic anomalies to the north and south. The spatial alignment between the local wind stress curl anomalies and the GS path suggests that NAO-related atmospheric forcing projects coherently onto the separated jet during this period. The negative wind stress curl anomalies over the GS path are expected to favor northward shifts in the GS path, through local anomalous Ekman pumping and the Rossby wave adjustment along the potential vorticity isolines set by the mean GS path (Frankignoul et al., 2001). The structure of the forcing along the mean GS axis is therefore consistent with the strong, positive NAO-GSI relationship observed during Period 1.

The regression of wind stress curl anomalies onto the GSI, with a lag of -8 months (i.e., changes in wind stress curl lead the GSI by 8 months), provides a dynamical link between the spatial pattern of wind stress curl forcing and the observed meridional displacements of the GS. During Period 1, the spatial organization of the lagged wind stress curl-GSI regression for the basin wide pattern (Figure 8c) as well as the local pattern (Figure 9c) closely resemble those of the wind stress curl-NAO regression (Figures 8a, 9a). This similarity (r = 0.91 and r = 0.94, for the basin and local scale wind stress curl-NAO and wind stress curl-GSI regression patterns, respectively) confirms that the dominant mode of wind stress curl forcing associated with the NAO is indeed the primary forcing pattern associated with meridional shifts in the GS path.

On the other hand, the intergyre-gyre structure is not found in Period 2; the spatial distribution of the wind stress curl anomalies associated with the NAO instead shift southwestward relative to Period 1 (Figure 8b), consistent with the southwestward shifts in the NAO centers of action identified in Section 3.3.1. The subpolar gyre is dominated by cyclonic (positive) wind stress curl anomalies, while the core of anticyclonic wind stress curl anomalies is now moved entirely into the subtropical gyre. This spatial pattern is consistent with the so-called gyre mode described by Häkkinen et al. (2011), a configuration more commonly associated with EAP-related variability than with the canonical NAO-related intergyre-gyre structure. The gyre mode is thought to modulate the strength of the subpolar and subtropical gyres, rather than the position of the gyre boundary, and is thus ineffective in driving shifts in the GS path, unlike the intergyre-gyre mode of Period 1.

At the local scale, wind stress curl anomalies are not spatially aligned well with the position of the mean GS in Period 2 (Figure 9b). Instead, alternating patches of cyclonic and anticyclonic wind stress curl anomalies appear along the mean GS path from west to east, with no apparent spatial organization over the separated current.

During Period 2, the lagged wind stress curl regression on GSI (Figure 8d) differs substantially from both the Period 1 wind stress curl-GSI pattern and the Period 2 wind stress curl-NAO pattern. The regression coefficients are overall weaker and the pattern is characterized by less spatial coherence. The overall pattern is negative over the subpolar gyre and positive in the eastern half of the subtropical gyre, which is weakly opposite to the wind stress curl-NAO pattern (Figure 8b). At the local scale (Figure 9b), the pattern is overall opposite to the corresponding local wind stress curl-NAO pattern (r = -0.56). The lack of spatial correspondence

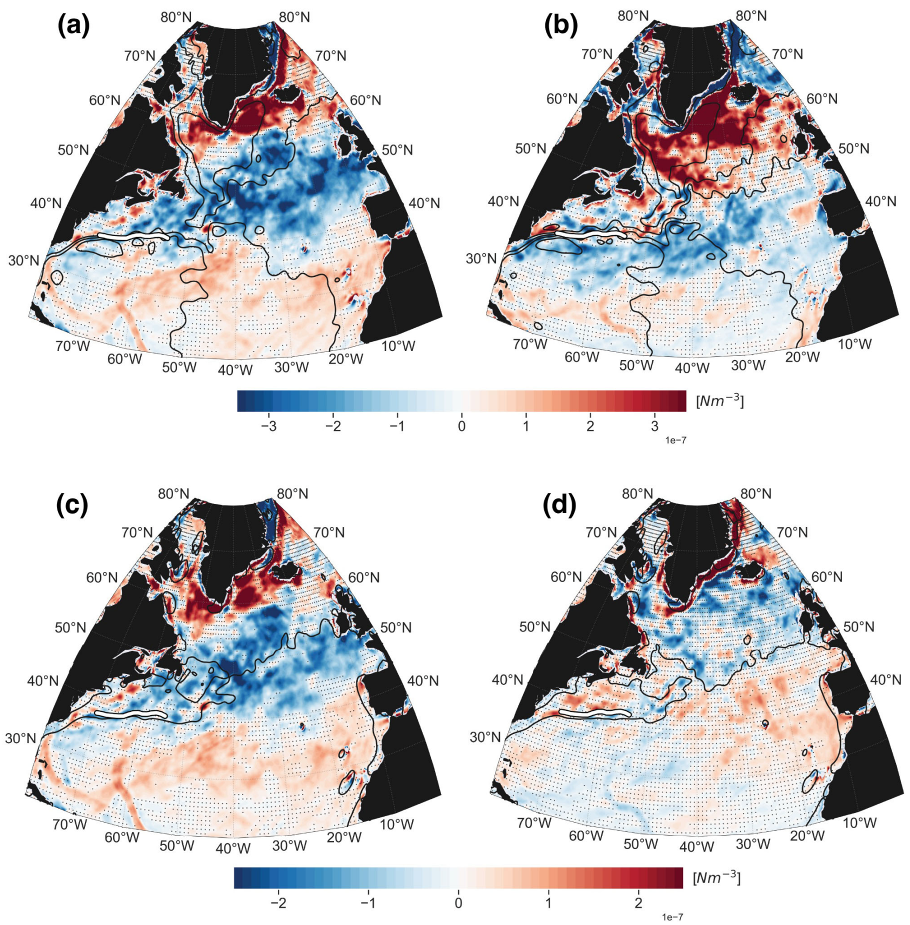

FIGURE 8
Regression of wind stress curl anomalies onto **(a, b)** NAO index and **(c, d)** observed GSI over North Atlantic for Period 1 [**(a, c)**; 1997–06 to 2001-10] and Period 2 [**(b, d)**]; 2004–02 to 2008-06]. Contours for **(a, b)** are mean sea surface height patterns for each period. Contours for **(c, d)** are the zero line of mean wind stress curl for each period. Stippled regions indicate regression slope is not significant at the 95% confidence level. Thick white line with black outline represents the mean path of the GS for the full record period (1993–01 to 2023-12).

between the wind stress curl-NAO and wind stress curl-GSI regressions in Period 2 (r = -0.26, for the basin scale) suggests that meridional displacements of the GS path are no longer dominantly associated with the wind stress curl pattern generated by NAO variability. Instead, GS displacements during this period appear to be associated with a more spatially complex and less organized wind-forcing field, consistent with the weakened and reversed NAO-GSI relationship observed during this interval.

Analogous regressions using the two-layer model GSI (not shown) are broadly consistent with the results described above. In Period 1, the lagged wind stress curl-GSI regression pattern closely resembles the NAO-related wind stress curl pattern shown in Figure 8a (r = 0.82 and r = 0.84 for the basin and local scale patterns, respectively). In Period 2, the lagged wind stress curl-GSI regression exhibits a similar spatial structure, but reverses sign relative to the NAO-related wind stress curl pattern in Figure 8b, but with opposite sign (r = -0.74 and r = -0.78 for the basin and local scale patterns, respectively). The reproduction of this sign reversal in the wind-driven model is consistent with the finding that changes in the wind forcing alone are sufficient to produce the observed reversal in the NAO–GSI relationship. The much stronger spatial correspondence between the wind stress curl-NAO and lagged wind stress curl-GSI regression patterns in the model compared to the observation (r = 0.74 versus r = 0.26 for the basin scale), and the stronger coherence of the wind stress curl-GSI in the two-layer model compared to the observations may reflect the contributions of additional processes in the observational forcing, which are absent from the wind-only two-layer model.

4 Discussion

The results presented here suggest that the non-stationarity of the NAO-GSI relationship appears to be closely associated with changes in the spatial structure of the atmospheric forcing and its alignment with the GS system and the gyre boundary, rather than from a fundamental change in the adjustment mechanism of the ocean circulation. EOF analysis demonstrates that the leading modes of sea level pressure variability represent dynamically evolving patterns rather than stationary modes of variability (Figures 3–7). The observed shifts in the NAO centers of action are accompanied by corresponding changes in the associated wind stress curl forcing (Figures 8a, b). Because western boundary

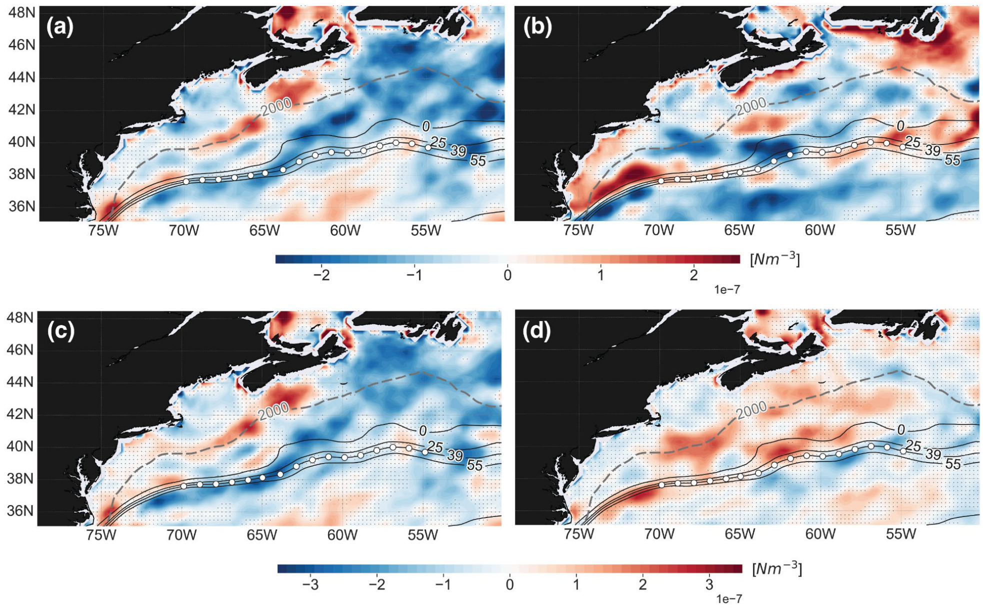

FIGURE 9
As in Figure 8, but for Gulf Stream region only. Solid black contours are isolines of mean sea surface height for the full record period (1993–01 to 2023-12). Dashed gray contours are the 2000m isobath. White dots represent the mean path of the GS for the full record period. Stippled regions indicate regression slope is not significant at the 95% confidence level.

current systems respond sensitively to the spatial distribution of atmospheric forcing, relatively modest shifts in the NAO dipole may substantially alter how NAO-related variability projects onto dynamically sensitive regions of the Northwest Atlantic.

The short time lag between the NAO and GS indices, together with the ability of the wind-driven two-layer model to reproduce the observed non-stationarity, provides evidence that wind forcing dominates the GS response to NAO at interannual timescales for most of the observational record. Because the two-layer model is driven by the full observed wind field, including changes in NAO amplitude, spatial structure, and other modes of atmospheric variability, the present simulatation does not isolate the effects of changes in NAO geometry alone. Rather, it demonstrates that wind forcing alone is sufficient to reproduce much of the observed non-stationarity. Although the present analysis does not uniquely identify the adjustment pathway responsible for the observed 8-month lag, the timescale itself provides useful insights into the underlying adjustment processes.

The canonical picture of the NAO-GS relationship describes a wind-driven mechanism, in which anomalous wind stress curl associated with the NAO generates sea surface height anomalies through Ekman pumping. When these sea surface height anomalies occur locally over the GS corridor, or propagate to the GS region as planetary Rossby waves, they modify the sea surface height gradients and pressure structure associated with the subtropical and subpolar gyres, resulting in meridional shifts of the GS path. In the classical framework, atmospheric forcing influences the GS through both a rapid local response over the western North Atlantic and a slower remote response involving westward-propagating Rossby waves generated in the central and eastern basin (Marshall et al., 2001).

The dominant lag between the observed NAO and GS response in the present study (8 months) falls between these canonical timescales, suggesting an adjustment mechanism that is neither purely local nor dominated by basin-crossing first-baroclinic Rossby waves. One possible explanation for this intermediate timescale is the excitation of topographic Rossby waves near the Tail of the Grand Banks of Newfoundland and along the continental slope, where NAO-related anticyclonic wind stress curl anomalies are comparable in magnitude to those observed in the central and eastern basin, regions commonly associated with Rossby wave generation in the canonical NAO-GS framework. Changes in large-scale wind forcing may generate pressure anomalies that propagate southwestward along continental slope toward the GS region. Such processes could provide a pathway by which NAO-related forcing influences the GS path on interannual timescales without requiring basin-wide baroclinic adjustment.

Another plausible mechanism that provides a fast GS path response to the wind stress curl changes is barotropic planetary Rossby wave adjustment. As the strong relative vorticity along the GS would deviate the background potential vorticity isolines from the constant latitudes, the GS path could act as a wave guide for both barotropic and baroclinic Rossby waves (c.f. Sasaki and Schneider, 2011). The positive sea level anomalies driven by the negative wind stress curl anomalies in the intergyre-gyre region may propagate as the barotropic Rossby waves along the GS wave guide and shift the GS northward, although the lag would be shorter than 8 months for this case. Similarly, a baroclinic Rossby wave along the GS wave guide originating within the 8-month range could contribute. The northward shift due to barotropic and baroclinic Rossby waves along the GS wave guide and that due to the topographic Rossby waves from the Tail of Grand Banks would work constructively, given the basin-scale spatial coherence of wind stress curl anomalies, particularly in Period 1.

While the wind-driven framework provides a consistent explanation for the dominant interannual GS response to NAO forcing over the full record and during Period 1, it does not appear to resolve all aspects of the observed GS response to NAO forcing during Period 2. This limitation is evident in both the performance of the wind-driven model and in the changing relationship between NAO-related wind stress curl and GS variability during this period. The wind-driven two-layer model reasonably reproduces the observed GSI prior to 2002, but the observed and modeled GSIs match poorly in Period 2 (r = -0.34, for filtered time series) compared to Period 1 (r = 0.66, for filtered time series; Figure 3a). In addition, if the non-stationary response of the GS were fully explained by the observed shifts in the geometry of the NAO-related wind forcing, we might expect the lagged wind stress curl-GSI regression during Period 2 (Figure 8d) to resemble the corresponding wind stress curl-NAO regression pattern (Figure 8b), with the altered projection of the forcing over the GS region producing a weakened or reversed response of the current relative to Period 1. Instead, the correspondence between these two regression fields weakens substantially during Period 2 (r = 0.91 for Period 1 and r = -0.26 for Period 2), suggesting that changes in the geometry of the NAO-related wind forcing alone are insufficient to explain the GS response during this period.

The apparent limitation of the wind-driven framework during Period 2 suggests that additional mechanisms may contribute to the observed GS response. One possible explanation is that buoyancy-driven variability contributes more strongly to the observed GS response during this interval. Because the evolving spatial structure of the NAO also modifies the associated surface buoyancy forcing, changes in both local and remote buoyancy forcing may contribute to the observed GS response. We briefly discuss the changes in the NAO-related surface turbulent heat flux forcing below, and believe that more thorough investigation on the role of the buoyancy forcing should be conducted in the future.

In addition to remote NAO-related buoyancy forcing originating in the subpolar North Atlantic, in particular the Labrador Sea, which would take much longer than 8 months to arrive, local buoyancy forcing may also impact the GS path. Frankignoul et al. (2001) identified positive SST anomalies near the GS preceding northward shifts of the GS by 0–20 months. These SST anomalies are generally associated with turbulent heat fluxes related to positive NAO phases (Deser et al., 2010; Hurrell and Deser, 2009). However, the strongest SST anomalies occurred in the slope water north of the GS axis at lag 8–12 months, suggesting more complex mechanisms than the direct response of the mixed layer to NAO buoyancy forcing. Because the spatial structure of the NAO changes substantially between Periods 1 and 2, the associated pattern of surface buoyancy forcing also change, both locally and remotely, potentially altering the response of the northern recirculation gyre and its influence on the separated GS (Figure 10).

The NAO-related turbulent heat flux regressions provide an opportunity to assess whether the evolving spatial structure of the NAO is accompanied by corresponding changes in surface buoyancy forcing. The wintertime (DJF) turbulent heat fluxes associated with the winter NAO over the full record exhibit the canonical tripolar structure (Cayan, 1992; Deser et al., 2010; Figure 10a), with the ocean losing heat to the atmosphere over the subpolar and tropical Atlantic and gaining heat in the middle latitudes. Enhanced heat loss over the Labrador Sea corresponds to the remote buoyancy pathway through which the NAO has been proposed to modulate the GS (Hameed and Piontkovski, 2004; Joyce et al., 2000; Pena-Molino and Joyce, 2008; Zhang and Vallis, 2007), while there is only weak downward heat flux anomalies north of the mean GS path. During Period 1, the large-scale NAO heat flux pattern broadly resembles the full-record regression, including enhanced heat loss over the subpolar gyre (Figure 10b). The structure of this pattern over the western North Atlantic, particularly in proximity to the GS, differs substantially, however: strong upward heat flux anomalies are found north of the mean GS path, while a broad region of anomalous downward heat flux extends into the central North

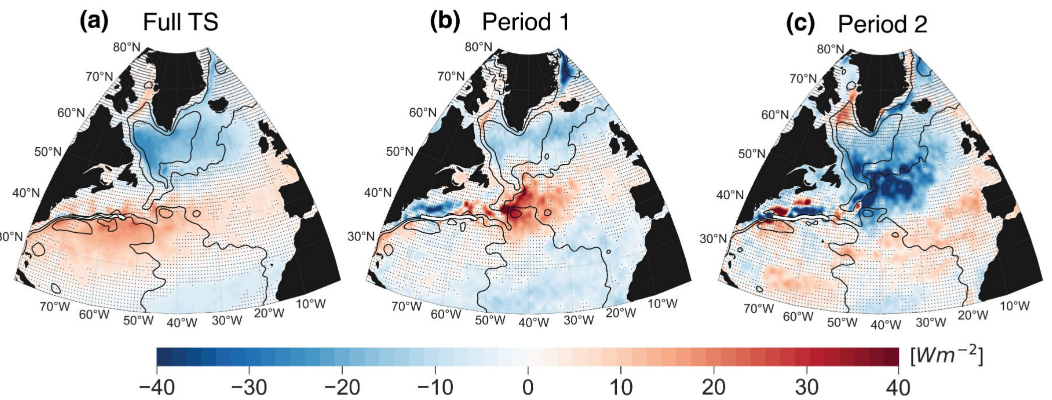

FIGURE 10
Regression of winter (DJF mean) turbulent heat flux (latent + sensible) onto winter (DJF mean) NAO index for **(a)** full time series (1993–01 to 2023-12), **(b)** Period 1 (1997–06 to 2001-10), and **(c)** Period 2 (2004–02 to 2008-06). Contours are isolines of mean sea surface height for each period. White line represent the mean path of the GS for the full record period. Stippled regions indicate regression slope is not significant at the 95% confidence level. The surface heat fluxes are positive downward (i.e., a positive flux indicates a flux from the atmosphere into the ocean).

Atlantic. During Period 2, the canonical tripolar NAO heat flux pattern is no longer evident (Figure 10c). Instead, the region of anomalous heat loss previously confined to the subpolar gyre expands and shifts southwestward, consistent with the southwestward displacement of the NAO centers of action. North of the mean GS path, there are large heat flux anomalies in alternating regions of upward and downward heat flux. It is noteworthy that the regions of strongest NAO-related heat flux anomalies are located much closer to the GS in both Periods 1 and 2 than in the full record, where the Labrador Sea exhibits strong heat flux anomalies.

The reorganization of the NAO-related turbulent heat flux field between Periods 1 and 2 shows that changes in the spatial structure of the NAO modify both local and remote buoyancy forcing. If the GS responds sensitively to the spatial distribution of buoyancy forcing, as it does to the spatial distribution of wind forcing, these changes could contribute to the altered NAO–GS relationship during Period 2. This possibility is also consistent with the divergence between the observed and modeled GSI time series beginning in the early 2000s, coincident with the transition to a weakened/reversed NAO–GSI relationship (Figure 3a). The secondary correlation peak observed when the NAO leads the GS by approximately 3–4 years (Figure 4), which is absent from the wind-driven model simulation, may likewise reflect the influence of a slower, buoyancy-driven adjustment processes, although the present analysis cannot distinguish this mechanism from other sources of low-frequency variability.

5 Summary and conclusions

While the relationship between the North Atlantic Oscillation (NAO) and the Gulf Stream (GS) has been the subject of extensive investigation for many decades, uncertainty remains regarding the mechanisms that govern the response of the GS to atmospheric variability, especially in terms of the dependence on the time scales and the periods of interest. This is particularly true in the context of the altimetry era (1993-present), over which the North Atlantic ocean has undergone rapid and unprecedented change (Saba et al., 2016). While the NAO-GS relationship has typically been regarded as quasi-linear and stationary, the evidence presented here demonstrates that both the strength and sign of this relationship can vary significantly with time, including at interannual time scales. Using satellite altimetry, atmospheric reanalysis, and a wind-driven two-layer model, we show that the NAO-GS relationship is non-stationary during the altimetric era, with both the sign and strength of the relationship varying at interannual timescales.

Analysis of the observed GS path and NAO indices reveals a statistically significant, positive correlation when the NAO leads the GS position by about 8 months. Moving correlation analysis demonstrates that this relationship is not stationary over the observational record, with a weaker but reversed relationship during the early 2000s. The ability of a wind-driven two-layer model to reproduce the timing and magnitude of this non-stationary behavior suggests that wind forcing plays a dominant role in governing the interannual NAO-GS relationship.

Comparison of atmospheric forcing patterns between periods of positive and negative NAO-GSI correlation demonstrates that the spatial structure of the NAO itself evolves substantially over the observational record. During the period of weakened and reversed NAO-GSI correlation, both the subtropical high and subpolar low shift southwestward relative to their mean positions. These shifts are accompanied by changes in the associated wind stress curl forcing and may alter how NAO-related atmospheric variability projects onto the GS system. During the period of strong positive correlation, coherent wind stress curl anomalies align closely with the GS path and northern recirculation gyre, producing a relatively direct and organized coupling between atmospheric variability and GS path shifts. During the period of weakened and reversed correlation, however, the forcing becomes displaced and spatially heterogeneous over the GS region, and the correspondence between NAO-related wind stress curl forcing and GS path variability breaks down.

Together, these results suggest that the observed non-stationarity is closely linked to changes in the spatial structure of the atmospheric forcing and its projection onto the background ocean circulation. While the short lead-lag relationships and wind-driven model results indicate that local wind forcing dominates the interannual response, the observed differences between the altimetric and wind-driven model records suggest that buoyancy-driven processes may also contribute depending on the time period. The mechanistic details of the buoyancy-driven GS path variability and its non-stationarity require further investigation in the future.

The results compiled here demonstrate the complexity of the relationship between large-scale atmospheric variability and the western boundary current system in the North Atlantic. While the canonical NAO-GS relationship described by Marshall et al. (2001) and others provides a foundation of dynamical understanding for the interactions within this system, it is important to consider the complexities in the system associated with changing oceanic and atmospheric conditions. In particular, we find that changes in the position and structure of the NAO appear to alter how wind stress curl anomalies project onto dynamically sensitive regions of the ocean, leading to unexpected variability in the oceanic response. This sensitivity has important implications for the predictability of the GS system and its downstream impacts on regional climate, sea level along the eastern North American margin, and marine ecosystems in the North Atlantic.

Data availability statement

The original contributions presented in the study are included in the article/Supplementary Material. Further inquiries can be directed to the corresponding author.

Author contributions

LE: Methodology, Validation, Conceptualization, Software, Resources, Investigation, Formal analysis, Writing – original

draft, Writing – review & editing, Visualization. Y-OK: Writing – review & editing, Methodology, Conceptualization, Supervision, Investigation, Funding acquisition. CF: Writing – review & editing, Investigation.

Funding

The author(s) declared that financial support was received for this work and/or its publication. NOAA Modeling, Analysis, Prediction and Projections Program (NA21OAR4310341) NSF Physical Oceanography Program (OCE-2219436).

Acknowledgments

The authors gratefully acknowledged the support from the NOAA Modeling, Analysis, Prediction and Projections Program (NA21OAR4310341) and NSF Physical Oceanography Program (OCE-2219436). We are very grateful to Dr. Jiayan Yang for sharing the two-layer wind-driven model simulation. We also wish to acknowledge helpful discussions with many colleagues including Drs. Isabela Le Bras, Glen Gawarkiewicz, Jaime Palter, and Abigail Bodner.

Conflict of interest

The author(s) declared that this work was conducted in the absence of any commercial or financial relationships that could be construed as a potential conflict of interest.

The reviewer YL declared a shared affiliation with the author LE to the handling editor at the time of review.

Generative AI statement

The author(s) declared that generative AI was not used in the creation of this manuscript.

Any alternative text (alt text) provided alongside figures in this article has been generated by Frontiers with the support of artificial intelligence and reasonable efforts have been made to ensure accuracy, including review by the authors wherever possible. If you identify any issues, please contact us.

Publisher's note

Supplementary material

The Supplementary Material for this article can be found online at: https://www.frontiersin.org/articles/10.3389/fmars.2026.1920990/full#supplementary-material

References

Cayan, D. R. (1992). Latent and sensible heat flux anomalies over the northern oceans: Driving the sea surface temperature. *J. Phys. Oceanogr.* 22, 859–881. doi: 10.1175/1520-0485(1992)022<0859:LASHFA>2.0.CO;2

Chassignet, E. P., Xu, X., Bozec, A., and Uchida, T. (2023). Impact of the new england seamount chain on gulf stream pathway and variability 53, 1871–1886. doi: 10.1175/JPO-D-23-0008.1

Chelton, D. B., and Schlax, M. G. (1996). Global observations of oceanic rossby waves. *Science* 272, 234–238. doi: 10.1126/science.272.5259.234

Chelton, D. B., deSzoeke, R. A., Schlax, M. G., Naggar, K. E., and Siwertz, N. (1998). Geographical variability of the first baroclinic rossby radius of deformation. *J. Phys. Oceanogr.* 28, 433–460. doi: 10.1175/1520-0485(1998)028<0433:GVOTFB>2.0.CO;2

Chen, L., Yang, J., and Wu, L. (2023). Topography effects on the seasonal variability of ocean bottom pressure in the north pacific ocean 53, 929–941. doi: 10.1175/JPO-D-22-0140.1

Deser, C., Alexander, M. A., Xie, S.-P., and Phillips, A. S. (2010). Sea surface temperature variability: Patterns and mechanisms. *Annu. Rev. Mar. Sci.* 2, 115–143. doi: 10.1146/annurev-marine-120408-151453

Dickson, R., Lazier, J., Meincke, J., Rhines, P., and Swift, J. (1996). Long-term coordinated changes in the convective activity of the north atlantic. *Prog. Oceanogr.* 38, 241–295. doi: 10.1016/S0079-6611(97)00002-5

Ebisuzaki, W. (1997). A method to estimate the statistical significance of a correlation when the data are serially correlated. *J. Clim.* 10, 2147–2153. doi: 10.1175/1520-0442(1997)010<2147:AMTETS>2.0.CO;2

Frankignoul, C., Coëtlogon, G., Joyce, T. M., and Dong, S. (2001). Gulf stream variability and ocean–atmosphere interactions. *J. Phys. Oceanogr.* 31, 3516–3529. doi: 10.1175/1520-0485(2002)031<3516:GSVAOA>2.0.CO;2

Gangopadhyay, A., Chaudhuri, A. H., and Taylor, A. H. (2016). On the nature of temporal variability of the gulf stream path from 75° to 55°w. *Earth Interact.* 20, 1–17. doi: 10.1175/EI-D-15-0025.1

Gangopadhyay, A., Cornillon, P., and Watts, D. R. (1992). A test of the parsons–veronis hypothesis on the separation of the gulf stream. *J. Phys. Oceanogr.* 22, 1286–1301. doi: 10.1175/1520-0485(1992)022<1286:ATOTPH>2.0.CO;2

Häkkinen, S., Rhines, P. B., and Worthen, D. L. (2011). Atmospheric blocking and atlantic multidecadal ocean variability. *Science* 334, 655–659. doi: 10.1126/science.1205683

Hameed, S., and Piontkovski, S. (2004). The dominant influence of the Icelandic low on the position of the gulf stream northwall. *Geophys. Res. Lett.* 31. doi: 10.1029/2004GL019561

Hersbach, H., Bell, B., Berrisford, P., Hirahara, S., Horányi, A., Muñoz-Sabater, J., et al. (2020). The ERA5 global reanalysis. *Q. J. R. Meteorolog. Soc* 146, 1999–2049. doi: 10.1002/qj.3803

Hong, B. G., Sturges, W., and Clarke, A. J. (2000). Sea level on the u.s. east coast: Decadal variability caused by open ocean wind-curl forcing. *J. Phys. Oceanogr.* 30, 2088–2098. doi: 10.1175/1520-0485(2000)030<2088:SLOTUS>2.0.CO;2

Hurrell, J. W. (1995). Decadal trends in the north atlantic oscillation: Regional temperatures and precipitation. *Science* 269, 676–679. doi: 10.1126/science.269.5224.676

Hurrell, J. W., and Deser, C. (2009). North atlantic climate variability: The role of the north atlantic oscillation. *J. Mar. Syst.* 78, 28–41. doi: 10.1016/j.jmarsys.2008.11.026

Joyce, T. M., Deser, C., and Spall, M. A. (2000). The relation between decadal variability of subtropical mode water and the north atlantic oscillation. *J. Clim.* 13, 2550–2569. doi: 10.1175/1520-0442(2000)013<2550:TRBDVO>2.0.CO;2

Joyce, T. M., Kwon, Y.-O., Seo, H., and Ummenhofer, C. C. (2019). Meridional gulf stream shifts can influence wintertime variability in the north atlantic storm track and Greenland blocking. *Geophys. Res. Lett.* 46, 1702–1708. doi: 10.1029/2018GL081087

Joyce, T. M., and Zhang, R. (2010). On the path of the gulf stream and the atlantic meridional overturning circulation. *J. Clim.* 23, 3146–3154. doi: 10.1175/2010JCLI3310.1

Kwon, Y.-O., Alexander, M. A., Bond, N. A., Frankignoul, C., Nakamura, H., Qiu, B., et al. (2010). Role of the gulf stream and kuroshio–oyashio systems in large-scale atmosphere–ocean interaction: A review. *J. Clim.* 23, 3249–3281. doi: 10.1175/2010JCLI3343.1

Le Bras, I. A.-A. (2023). Labrador sea water spreading and the atlantic meridional overturning circulation. *Philos. Trans. R. Soc. A. Mathematical Phys. Eng. Sci.* 381, 20220189. doi: 10.1098/rsta.2022.0189

Lee, T., and Cornillon, P. (1995). Temporal variation of meandering intensity and domain-wide lateral oscillations of the gulf stream. *J. Geophysical Research: Oceans* 100, 13603–13613. doi: 10.1029/95JC01219

Marshall, J., Johnson, H., and Goodman, J. (2001). A study of the interaction of the north atlantic oscillation with ocean circulation. *J. Clim.* 14, 1399–1421. doi: 10.1175/1520-0442(2001)014<1399:ASOTIO>2.0.CO;2

Nye, J. A., Joyce, T. M., Kwon, Y.-O., and Link, J. S. (2011). Silver hake tracks changes in northwest atlantic circulation. *Nat. Commun.* 2, 412. doi: 10.1038/ncomms1420

Paolini, L. F., Omrani, N.-E., Bellucci, A., Athanasiadis, P. J., Ruggieri, P., Patrizio, C. R., et al. (2024). Nonstationarity in the NAO–gulf stream SST front interaction. *J. Clim.* 37, 1629–1650. doi: 10.1175/JCLI-D-23-0476.1

Pena-Molino, B., and Joyce, T. (2008). Variability in the slope water and its relation to the gulf stream path. *Geophys. Res. Lett.* 35. doi: 10.1029/2007GL032183

Pérez-Hernández, M. D., and Joyce, T. M. (2014). Two modes of gulf stream variability revealed in the last two decades of satellite altimeter data. *J. Phys. Oceanogr.* 44, 149–163. doi: 10.1175/JPO-D-13-0136.1

Saba, V. S., Griffies, S. M., Anderson, W. G., Winton, M., Alexander, M. A., Delworth, T. L., et al. (2016). Enhanced warming of the northwest atlantic ocean under climate change. *J. Geophysical Research: Oceans* 121, 118–132. doi: 10.1002/2015JC011346

Sanchez-Franks, A., Hameed, S., and Wilson, R. E. (2016). The Icelandic low as a predictor of the gulf stream north wall position. *J. Phys. Oceanogr.* 46, 817–826. doi: 10.1175/JPO-D-14-0244.1

Sasaki, Y. N., and Schneider, N. (2011). Interannual to decadal gulf stream variability in an eddy-resolving ocean model. *Ocean Modell.* 39, 209–219. doi: 10.1016/j.ocemod.2011.04.004

Silver, A., Gangopadhyay, A., Gawarkiewicz, G., Taylor, A., and Sanchez-Franks, A. (2021). Forecasting the gulf stream path using buoyancy and wind forcing over the north atlantic. *J. Geophysical Research: Oceans* 126, e2021JC017614. doi: 10.1029/2021JC017614

Spall, M. A. (1996). Dynamics of the gulf stream/deep western boundary current crossover. part II: Low-frequency internal oscillations. *J. Phys. Oceanogr.* 26, 2169–2182. doi: 10.1175/1520-0485(1996)026<2169:DOTGSW>2.0.CO;2

Talley, L. D. (1996). North atlantic circulation and variability, reviewed for the CNLS conference. *Physica D. Nonlinear Phenomena* 98, 625–646. doi: 10.1016/0167-2789(96)00123-6

Taylor, A. H., and Gangopadhyay, A. (2001). A simple model of interannual displacements of the gulf stream. *J. Geophysical Research: Oceans* 106, 13849–13860. doi: 10.1029/1999JC000147

Taylor, A. H., and Stephens, J. A. (1998). The north atlantic oscillation and the latitude of the gulf stream 50, 134. doi: 10.3402/tellusa.v50i1.14517

Wolfe, C. L. P., Hameed, S., and Chi, L. (2019). On the drivers of decadal variability of the gulf stream north wall. *J. Clim.* 32, 1235–1249. doi: 10.1175/JCLI-D-18-0212.1

Yang, J. (2015). Local and remote wind stress forcing of the seasonal variability of the atlantic meridional overturning circulation (AMOC) transport at 26.5°n. *J. Geophysical Research: Oceans* 120, 2488–2503. doi: 10.1002/2014JC010317

Yang, J., and Chen, K. (2021). The role of wind stress in driving the along-shelf flow in the northwest atlantic ocean. *J. Geophysical Research: Oceans* 126, e2020JC016757. doi: 10.1029/2020JC016757

Zhang, R., and Vallis, G. (2007). The role of bottom vortex stretching on the path of the north atlantic western boundary current and on the northern recirculation gyre. *J. Phys. Oceanogr.* 37, 2053–2080. doi: 10.1175/JPO3102.1

Supplementary Material

1 SUPPLEMENTARY FIGURES

1.1 Figures

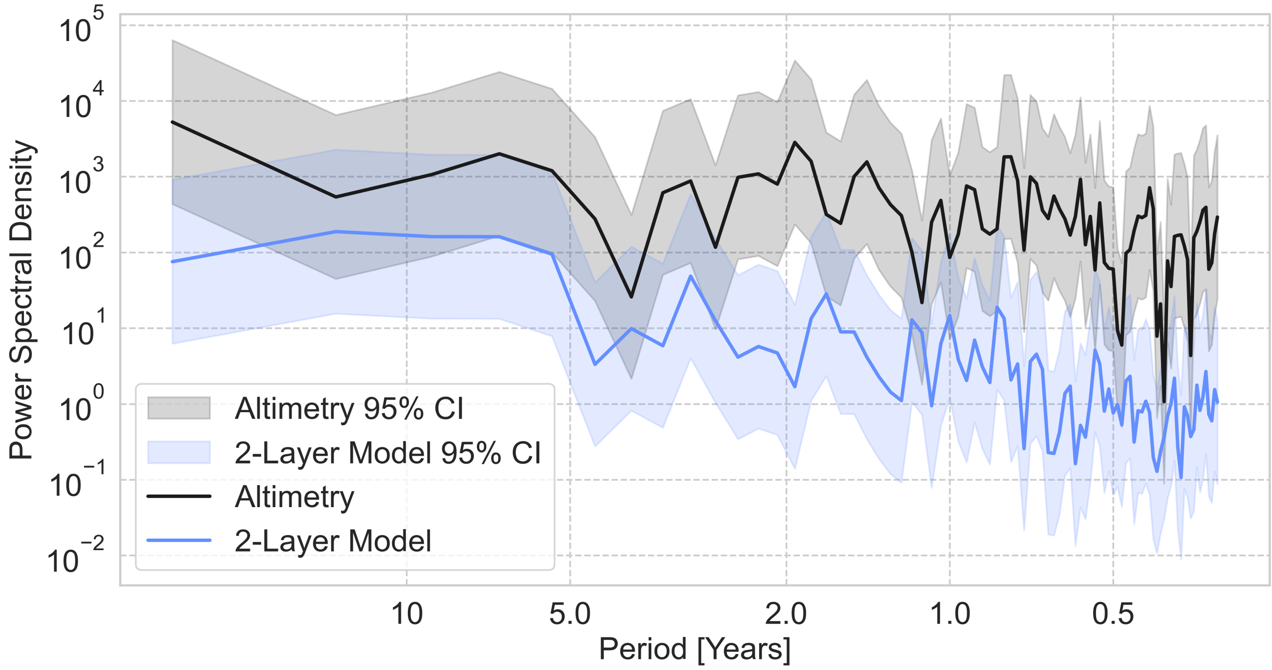

Figure S1. Power spectra of observed (black) and two-layer model (blue) Gulf Stream Index (GSI) time series. Shading indicates 95 % confidence interval.

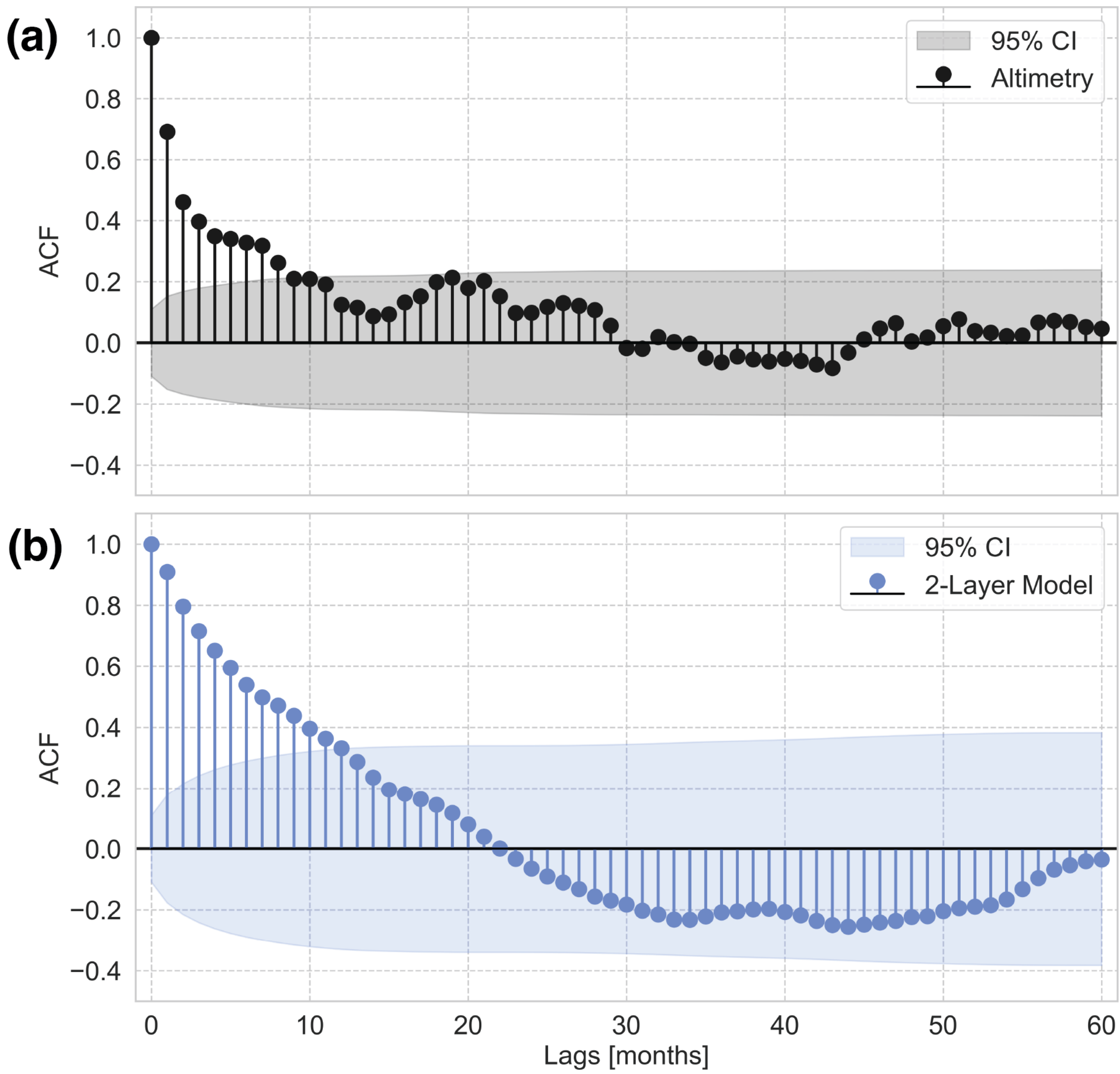

Figure S2. Autocorrelation functions for (a) observational and (b) two-layer model GSI time series. Shading indicates 95 % confidence interval.

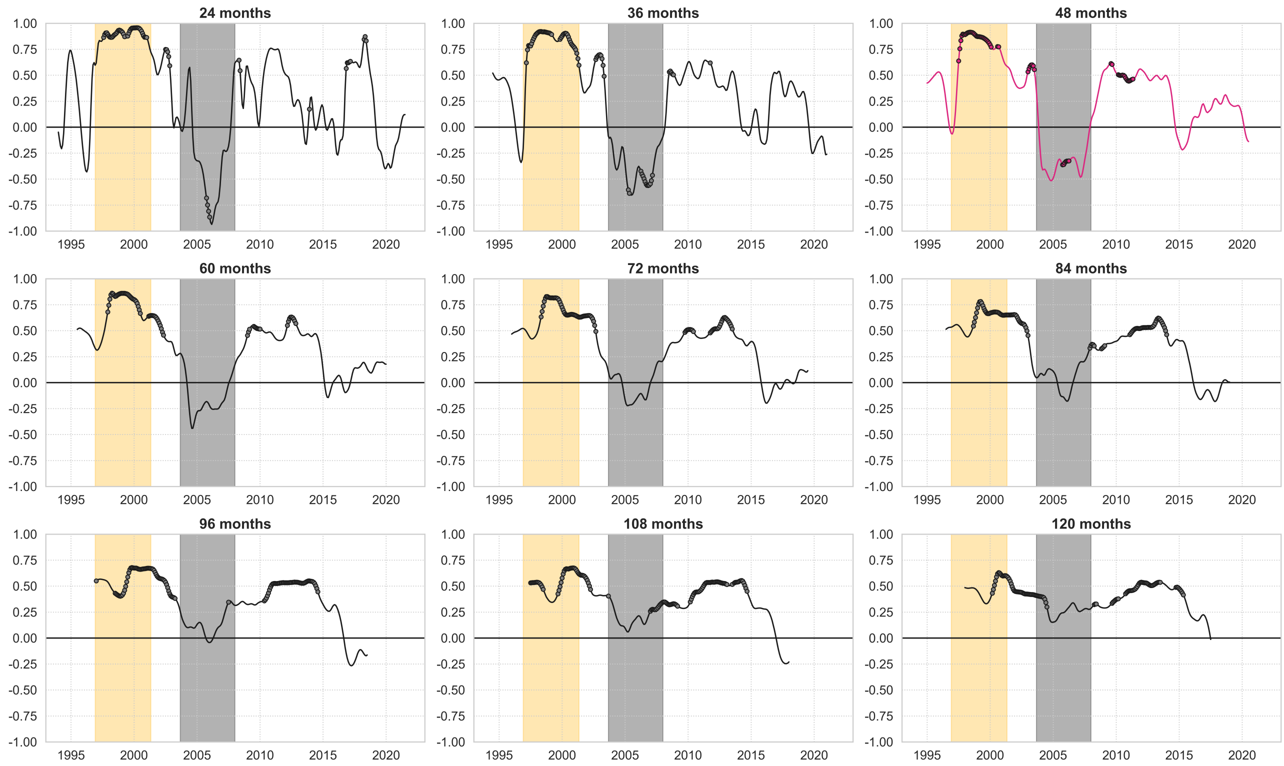

Figure S3. Sensitivity of observed GSI-NAO moving correlation to moving window size. Window sizes ranging from 24 months (top left) to 120 months (bottom right) were tested, each with a fixed lag of -8 months. Dots represent correlations that are statistically significant at the 95 % confidence level. The selected window size of 48 months is shown in pink (top right).

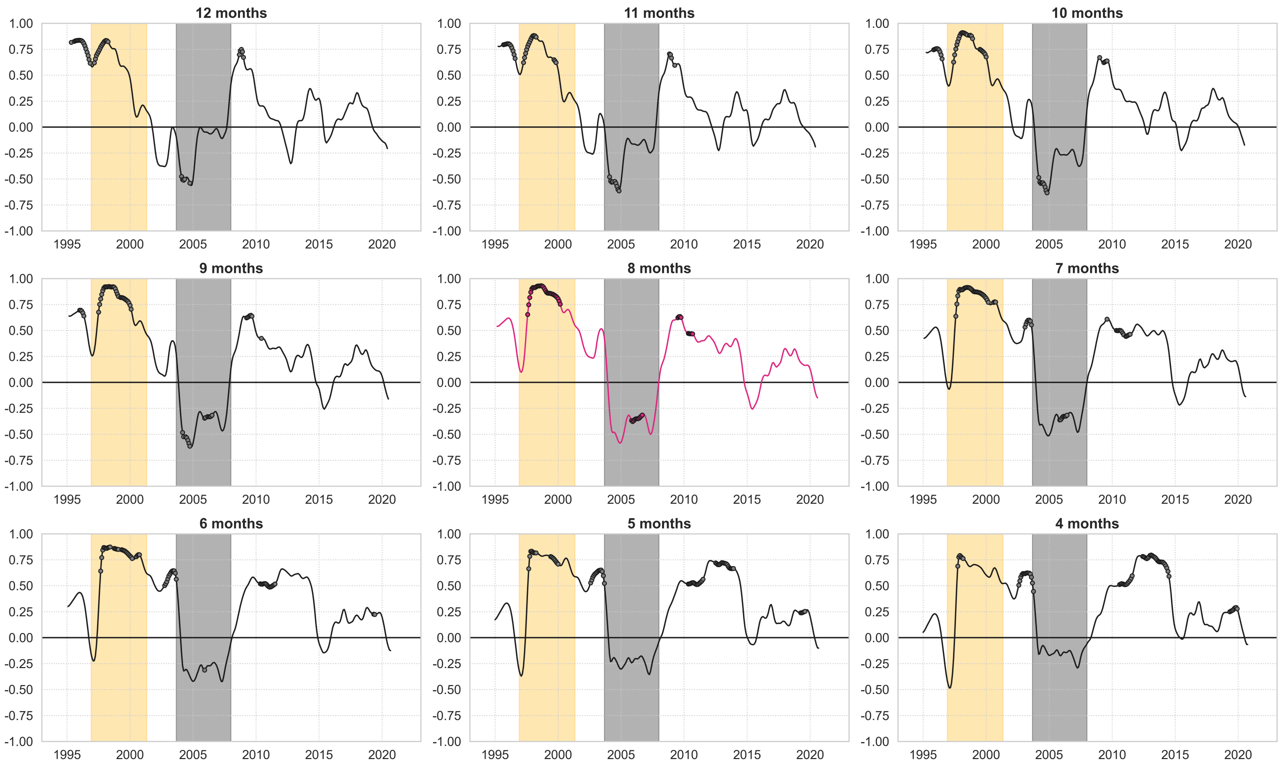

Figure S4. Sensitivity of observed GSI-NAO moving correlation to GS lag. Lags ranging from -12 (top left) months to -4 months (bottom right) were tested, each with a fixed window size of 48 months. Dots represent correlations that are statistically significant at the 95 % confidence level. Note that all lags tested represent GS lagging NAO (i.e., negative lags corresponding to Figure 4). Positive values are reported in figure titles for clarity. The selected window size of 8 months is shown in pink (center).

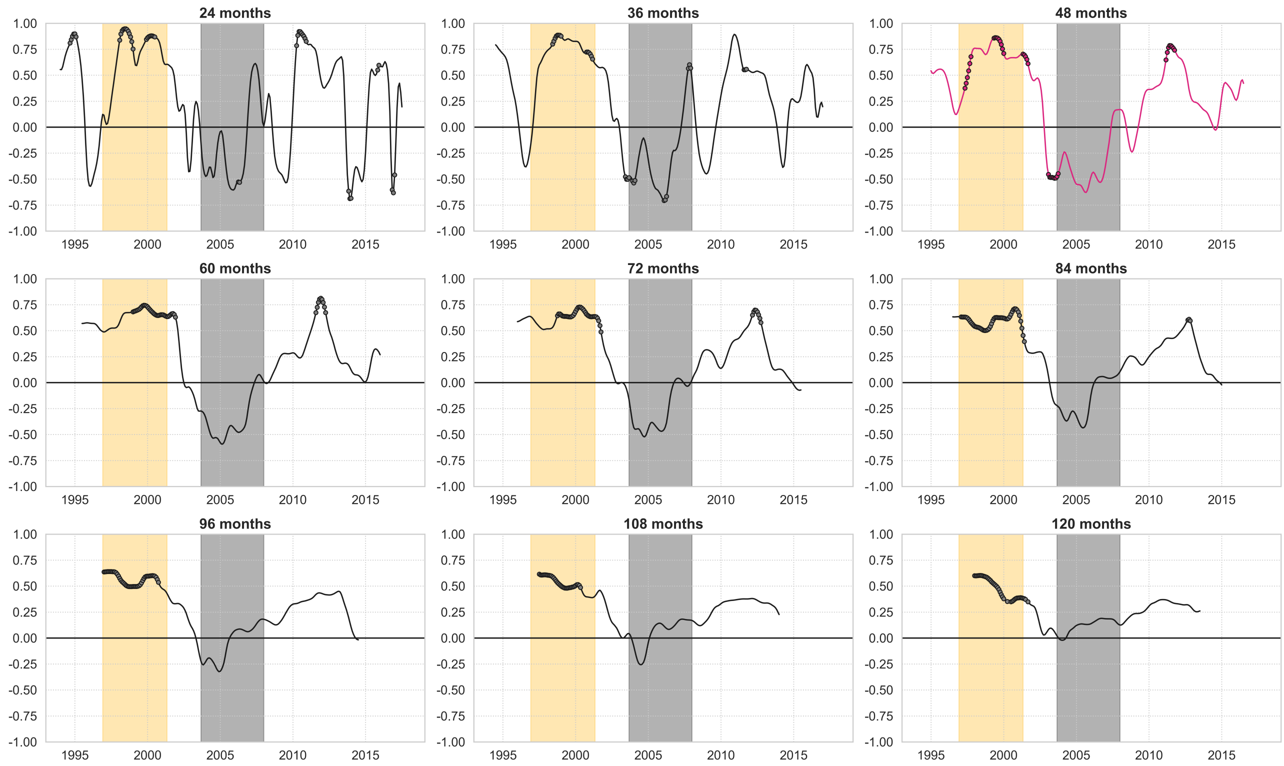

Figure S5. Sensitivity of two-layer model GSI-NAO moving correlation to moving window size. Window sizes ranging from 24 months (top left) to 120 months (bottom right) were tested, each with a fixed lag of -2 months. Dots represent correlations that are statistically significant at the 95 % confidence level. The selected window size of 48 months is shown in pink (top right).

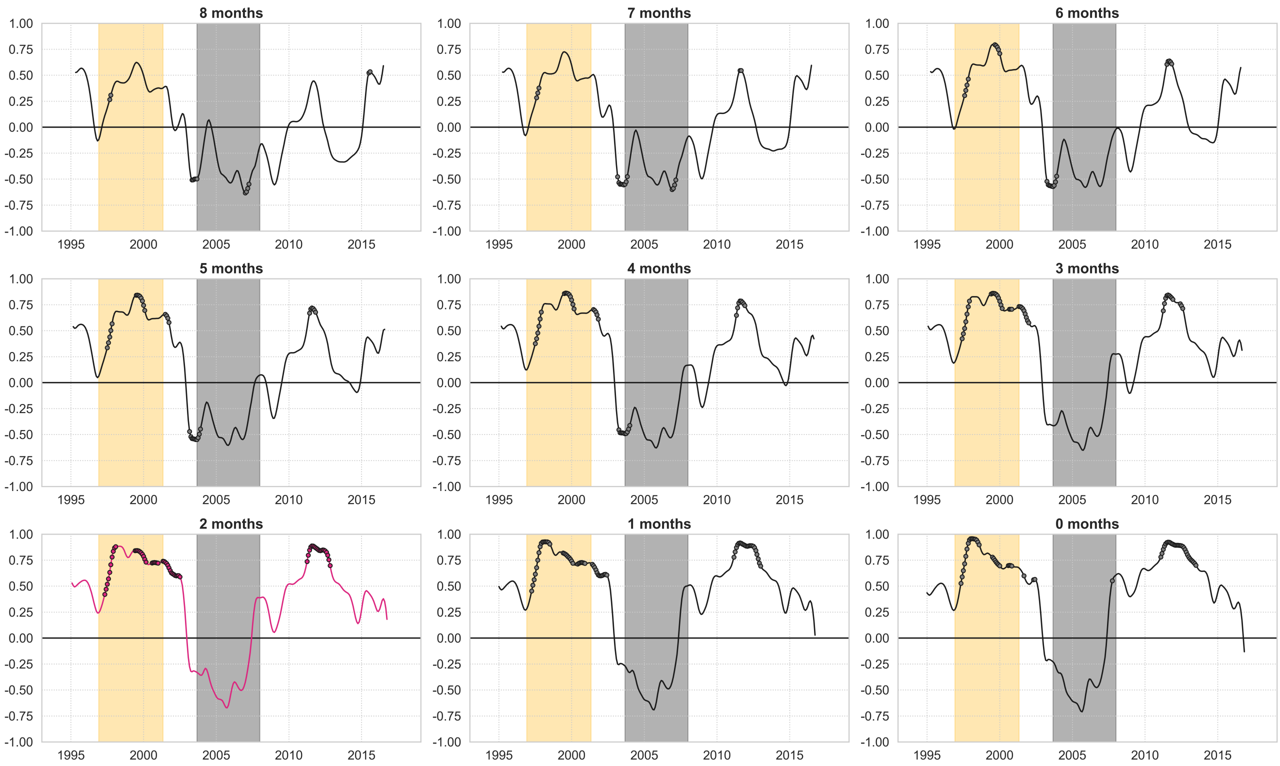

Figure S6. Sensitivity of two-layer model GSI-NAO moving correlation to GS lag. Lags ranging from -8 (top left) months to 0 months (bottom right) were tested, each with a fixed window size of 48 months. Note that all lags tested represent GS lagging NAO (i.e., negative lags corresponding to Figure 4). Positive values are reported in figure titles for clarity. Dots represent correlations that are statistically significant at the 95 % confidence level. The selected window size of 2 months is shown in pink (bottom left).